Enríquez, E., Fuertes, V., Cabrera, M. J., Seores, J., Muñoz, D., Galiana, B., & Fernández, J. F. (2019). Study of the crystallization in fast sintered Na-rich plagioclase glass-ceramic. *In Ceramics International, 45*(7), 8899–8907

DOI:10.1016/j.ceramint.2019.01.219

Ceramics International xxx (2019) xxx-xxx

Contents lists available at ScienceDirect

Ceramics International

journal homepage: www.elsevier.com

Study of the crystallization in fast sintered Na-rich plagioclase glass-ceramic

E. Enríquez[a, *, 1], V. Fuertes[b, 1], M.J. Cabrera[a], J. Seores[a], D. Muñoz[a], B. Galiana[c], J.F. Fernández[b]

[a] Centro tecnológico Vidres, S.L., Ctra. Onda, Km 3.4, 12540, Villareal, Castellón, Spain
[b] Electroceramics Department, Instituto de Cerámica y Vidrio, CSIC, Kelsen 5, 28049, Madrid, Spain
[c] Physics Department, Universidad Carlos III de Madrid, Av. Universidad 40, 28911, Leganés, Madrid, Spain

ARTICLE INFO

Keywords:
Glass-ceramic
Plagioclase feldspar
Micro-nanostructure
Crystallization processes
Fast sintering

ABSTRACT

A dense, ~94% of crystalline phase, glass-ceramic based on Na-rich plagioclase feldspar crystallizations has been obtained by a fast sintering process for the first time. By using Sr^{2+} and Ca^{2+} as nucleating agents, a unique hierarchical micro-nanostructure is developed in a fast sintering process at 1220 °C. In this work, a thorough study about crystallization processes of this novel material has been extensively carried out through thermal quenching experiments and supported by DTA/TG, Hot stage microscopy, XRD, FE-SEM, TEM/HRTEM and XPS measurements. The study reveals that crystallization takes place in two steps during the sintering process. Microcrystals nucleate on heating at temperatures >900 °C, while nanocrystals start nucleating at the dwelling temperature, 1220 °C. However, it is during holding and cooling time when nanostructures zones grow, and the unique highly crystalline micro-nanostructure is developed. Structural and compositional analysis supported by NMR, shows the main presence of Q_4(nAl) albite-like sites and in lesser extent anorthite-like sites, corroborating the formation of a sodic plagioclase structure. The analysis of Si neighbours indicates that chemical environment presents a slight Si/Al disorder at short range.

1. Introduction

Feldspars are widely used in ceramic industrial applications, due to their high alumina content and its abundance in the earth's crust. Most of the products used on a daily basis are made with feldspar raw materials, such as glass for protection, fiberglass for insulation, floor tiles and tableware, among others. Feldspars are very interesting natural mineral due to their excellent properties, such as high Mohs hardness and chemical inertness. Feldspars are basically classified into two groups, plagioclases and alkali feldspars. The first one is a solid solution between albite ($NaAlSi_3O_8$) and anorthite ($CaAl_2Si_2O_8$) end members, while the second one is a solid solution between K-feldspars ($KAlSi_3O_8$) and albite. Feldspars are usually integrated in igneous rocks and, therefore, they have many impurities and intermediate compositions. Feldspar synthesis is still a challenge to obtain pure phase materials under controlled conditions to tailor properties [1–3].

The crystallization processes are of great relevance in the feldspar synthesis. In magmatic rocks, crystallization strongly depends on the cooling rate, pressure, geological time and the abundance of liquid media. The presence of high amount of water can produce great compositional changes in the feldspars minerals [4]. Feldspar synthesis based on hydrothermal process is commonly attempt to obtain pristine particles with complex processes [5–8]. The sol-gel methods are also used to synthesize crystalline feldspar particles [9]. The most common way to synthetize feldspars is following the ceramic procedure of frits. A frit is a ceramic composition that has been melted in a special melting oven and quenched to form a glass. However, the further thermal treatment of frits developed a typical porcelain structure in which feldspar crystallization occurs in a continuous glassy matrix [1,2]. Feldspars find several difficulties to crystallizes from its melts, and thus, the use of seeds is usually necessary to produce feldspars by this route [4,10]. The processing route became more complex when a high crystalline glass-ceramic is pursuit, since larger thermal treatments are required and in some extent it is combined with vacuum systems [2,11].

A glass-ceramic material is usually obtained by controlled devitrification process, which consists in cooling a glass below its melting temperature, in which a nucleation process is produced followed by crystal growth. Sometimes, nucleation and crystallization can coexist when their corresponding temperatures are close enough. In these situ-

* Corresponding author.
Email address: esther@icv.csic.es (E. Enríquez)
[1] These authors contributed equally to this work.

https://doi.org/10.1016/j.ceramint.2019.01.219
Received 29 November 2018; Received in revised form 25 January 2019; Accepted 28 January 2019
Available online xxx

ations, the glass-ceramic formation is optimum, since there is a large presence of nuclei where the crystals can grow, creating a fine microstructure. The crystal growth rate strongly depends on the fusion entropy that for anorthite, albite and orthoclase are 72.2, 46.3 and 36.0 J/Kmol, respectively [12]. Therefore, Albite feldspar has quite lower crystal growth rate ($\approx 10^{-10}$ ms^{-1}) than anorthite ($\approx 10^{-4}$ ms^{-1}). Moreover, albite crystal growth is produced at lower range of temperatures (1000-1100 °C) regarding anorthite (1200-1300 °C). These characteristics make it necessary to use nucleating agents to accelerate the crystallization process of the albite. The presence of nucleating agent in form of seeds would produce an heterogeneous nucleation due to larger amount of boundaries [4,13]. However, it was demonstrated that ZrO_2 seeds do not favor the crystallization of albite feldspars [14]. On the other hand, selected cations as Zr, Ca or Sr, can act as nucleating agents following a homogeneous nucleation process. Albite feldspar is an alkali aluminosilicate quite difficult to obtain as single phase, both naturally and synthetically, since the presence of other cations apart from Na^{1+}, such as Ca^{2+} and K^{1+}, favors the simultaneous formation of anorthite and orthoclase feldspars, respectively. For these reason, the use of seeds having isomorphs crystal structure than albite, such as anorthite, is often needed [4,13,15]. Besides, Sr^{2+} can act as nucleating agent to form strontium feldspar ($SrAl_2Si_2O_8$) which would favor the albite or anorthite crystallization. However, in the anorthite crystallization is less probable since it requires higher temperatures, ~1400 °C [12]. An approximation to the problem may be to deal with sodic plagioclases that are materials which present albite as a major component and anorthite as minor one. Recently, a high dielectric strength response of albite-based glass-ceramics is reported [16]. The excellent insulator properties are based on their unique micro-nanostructure that consists of isolated micrograins surrounded by nanostructured regions forming a hierarchical microstructure. Such hierarchical microstructure serves to tailor properties of the glass-ceramics as thermal diffusivity [15] and wear resistance [17].

Thus, in this work, the objective is to study the crystallization process that occurs in synthetic plagioclase-based glass-ceramic with high albite content processed by a fast sintering process. The glass-ceramic materials are obtained from a glass frit. With the aim of deepening in the heating and cooling steps and therefore, in crystallization and devitrification process, DTA/TG and quenching experiments were carried out. Compositional and microstructural analysis of quenched and sintered samples by XRD, FE-SEM, TEM and HRTEM is combined with structural characterization by XPS and NMR and reveals that crystallization of the Na-rich plagioclase occurs in two steps.

2. Experimental procedure

2.1. Sample preparation

The glass ceramic based on Na-rich plagioclase feldspar was prepared following a fast sintering process easily adaptable for the tile industry [18,19]. Firstly, a composition melted in a furnace at 1450-1500 °C and then, water quenched to form the frit precursor. Once obtained the frit, it was homogenized with kaolin (Molcasa) in a weight proportion 90/10, in an alumina ball miller during 20 min with 37 wt% of water. Then, the resulted material was dried in an oven at 80 °C and sieved by a 63 μm sieve. The powder obtained was pressed in pellets of ~10 mm in thickness, at 400 kg/cm^2 of pressure. Finally, samples were thermally treated in an industrial furnace at 1220 °C with dwelling time of 6 min with a heating and cooling rate of 30 °C/min. The composition of the final material is expressed in term of equivalent oxides in Table 1. The minority components of the composition (providing from the raw materials) having concentrations < 1 wt% (B_2O_3, TiO_2, P_2O_5, Fe_2O_3, MgO, BaO, ZnO) are included in the term "others".

In order to study the crystallization degree during the densification process at selected temperatures, a thermal quenching process was carried out. For this purpose, powder pellets were prepared following the procedure explained above, and they were heated up to 800 °C, 900 °C, 1100 °C and 1200 °C, temperatures at which the sample was extracted and immersed quickly in cold water to freeze the structure obtained at those temperatures.

2.2. Characterization

Thermal behavior of the glass-ceramic was studied by means of differential thermal analysis (DTA) and thermogravimetric (TG) analysis using a Thermo-Analyzer Netzch STA 409 with a temperature controller Netzch TASC 414/2 being the reference α-Al_2O_3. Hot-stage microscopy was also carried out by a Leica Leitz microscope. Both measurements were made in the range 30–1250 °C with a heating rate of 10 °C/min in air atmosphere.

Microstructural characterization was studied by means of Field Emission Scanning Electron Microscopy (FESEM) using a Hitachi S-4700. Polished samples were chemically etched with 5 vol% of HF with the aim of removing the glassy phase to reveals the microstructure. In addition, the crystalline phases formed were identified by using X-ray diffraction (XRD) technique in a diffractometer Bruker D8 Advance with Cu Kα radiation, 40 kV and 40 mA, in sintered samples. The identification of the crystalline phases was carried out by the comparison with the JCPDS patterns, and the glassy phase content was obtained through the integration of the areas corresponding to the glassy and crystalline phases by means of the diffraction software Bruker's Diffrac.Eva.

Transmission electron microscopy (TEM) was performed at 200 keV on Philips Tecnai F20. Samples were prepared in cross-section by standard sample preparation methods, mechanical thinning and argon ion milling to electron transparency. High resolution TEM (HRTEM) images were also acquired to study the local crystalline quality. Electron diffraction pattern and diffraction pattern simulations after fast Fourier transform (FFT) of HRTEM images were also used.

X-ray photoelectron spectroscopy (XPS) was carried out by an X-ray photoelectron spectrometer (XPS, K-Alpha, Thermo Scientific). Samples were deeply polished before measuring in order to be able to study the internal part of the materials. Prior to analysis, the samples were cleaned by ion bombardment with an Ar^+ beam (2 kV) for 5 min. A monochromatic Al K_α (1486.6 eV) source running at a voltage of 12 kV with a pass energy of 40 eV was used for high-resolution region scans and 200 eV for survey scans; finally, for charge correction a 1 point scale with the C 1s peak shifted to 284.60 eV was used.

Structural characterization at short range was made by solid state MAS nuclear magnetic resonance (NMR) on the powders obtained by milling the sintered samples at room temperature. ^{29}Si MAS NMR spectra were recorded on a Bruker AV-400-WB spectrometer equipped with 4 mm MAS probe and operating at 79.49 MHz by a simple pulse

Table 1
Composition of studied glass ceramic and glaze expressed as equivalent oxides. The minority components are all included in others (B_2O_3, TiO_2, P_2O_5, Fe_2O_3, MgO, BaO, ZnO).

Oxides wt. %	SiO_2	ZrO_2	Al_2O_3	CaO	Na_2O	SrO	K_2O	ZnO	Others
Frit	54.67	1.24	22.63	7.73	2.14	7.20	1.44	1.27	2.96
Kaolin	55.49	–	42.48	0.17			1.21		0.65

of π/2 at 50 KHz. Relaxation time was of 60s, spectral width of 40 kHz and 2 h of accumulation time with a spinning rate of 10 kHz were taken. Kaolin (−91.2 ppm) was used as secondary reference with respect to TMS as primary reference.

3. Results and discussion

3.1. Thermal evolution of the crystallization in Na-rich plagioclase glass-ceramic formation

In order to analyze the thermochemical reactions that occurs during the thermal treatment firstly, DTA-TG measurements and hot stage microscopy of the frit and kaolin mixture were made (Fig. 1a and b, respectively. DTA-TG results reveal two endothermic peaks related to the adsorbed water loss up to ~150 °C (region 1) and organic-based processing additives that burn out from 300 °C to 400 °C with an associated weight loss of 0.5% (region 2). A relevant endothermic peak is observed at ≈500 °C (region 3) corresponding to the structural water dihydroxylation of Kaolin that transform into metakaolin along with a mass loss of ≈2% [20]. Also associated with metakaolin, an exothermic peak appears at ≈900 °C (region 4), which corresponds to an aluminum-silicon spinel or pre-mullite type crystals attributed to a transformation of the SiO4 groups combine with the AlO6 groups to form the Al—Si spinel phase, precursor of the mullite phase [21,22]. Finally, an exothermic process corresponding to the albite-rich feldspar crystallization occurs at ≈1040 °C (region 5). These two exothermic processes correlated with crystallizations do not have associated a loss of weight. In addition, the cooling curve is also measured in order to check if any thermal or structural process occurs during this period. However, the resolution obtained does not reveal any significant process and the curve is omitted.

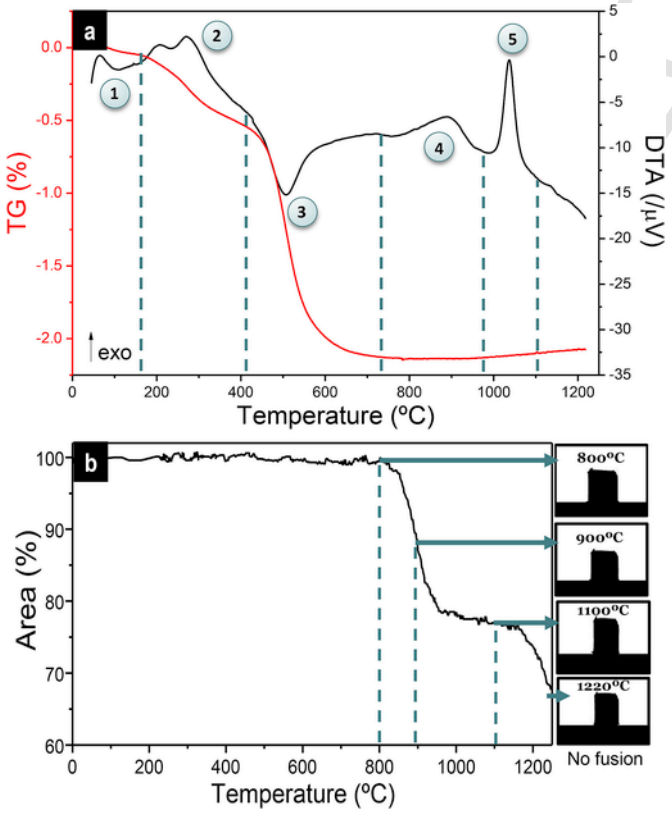

Fig. 1. a) DTA-TG of frit - kaolin (90%–10%) mixture from room temperature (RT) to 1220 °C; b) Hot stage microscopy of this material in the same temperature range of a).

According to this information, hot stage microscopy is carried out from room temperature up to 1220 °C, in order to determine the influence of different thermal processes of the Na-rich feldspar formation (Fig. 1b). At 800 °C it is possible to observe the beginning of the first material shrinkage, with a 13% of reduction of its effective area, up to 900 °C. At 800 °C the glaze powders started to shrink with a low rate, indicating a mechanism associated with low mass transport due to the reaction of the metakaolin with the particles of frit [20]. The shrinkage rate decreases drastically at 960 °C, indicating a change of the mass transport mechanism. The decreasing of shrinkage rate in glaze materials is typical of the appearance of crystalline phase that evolved from the glassy phase. The devitrification of frit particles seems to be in the origin of such change. At 1150 °C the material begins to soften, however, as it is seen in the hot stage microscopy image the material does not melt in the studied temperature range.

Therefore, attending to these results, the temperatures of interest defined for specific thermally treatments and thermal quenching are 800 °C (beginning of the process), 900 °C (in the middle of the sintering process), 1100 °C (crystallization range) and 1220 °C (before the melting point). The samples obtained are structurally characterized by XRD (Fig. 2) and microstructural analyzed by FESEM (Fig. 3). Quenched samples are compared with the material sintered at 1220 °C with a dwell time of 6 min.

The XRD patterns (Fig. 2) show that a thermal treatment up to 900 °C the material is still amorphous presenting a wide band at low 2θ angles, and quartz (JCPDS card no. 00-046-1045) traces as crystalline phase. This quartz trace comes from the kaolin raw material. Hence, at these temperatures, the frit is still in the vitreous phase and the nucleation and crystallization of the glasses have not occurred. At 1100 °C, the slowest shrinkage rate temperature range during the sintering observed in the hot stage microscopy curve, the plagioclase crystallization has already produced, and it is possible to observe the well-defined XRD pattern (JCPDS card no. 00-041-1480), with very low amount of glassy phase. In addition, other minority phases appear: zircon (JCPDS card no. 00-003-064), quartz (JCPDS card no. 00-046-

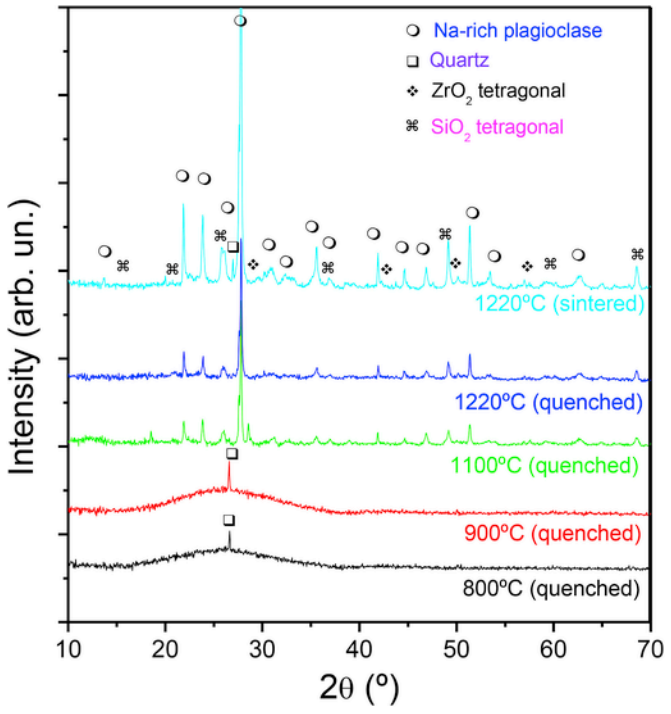

Fig. 2. XRD pattern of the quenched samples at 800 °C, 900 °C, 1100 °C and 1220 °C in comparison with the sample sintered at 1220 °C with a dwell time of 6 min.

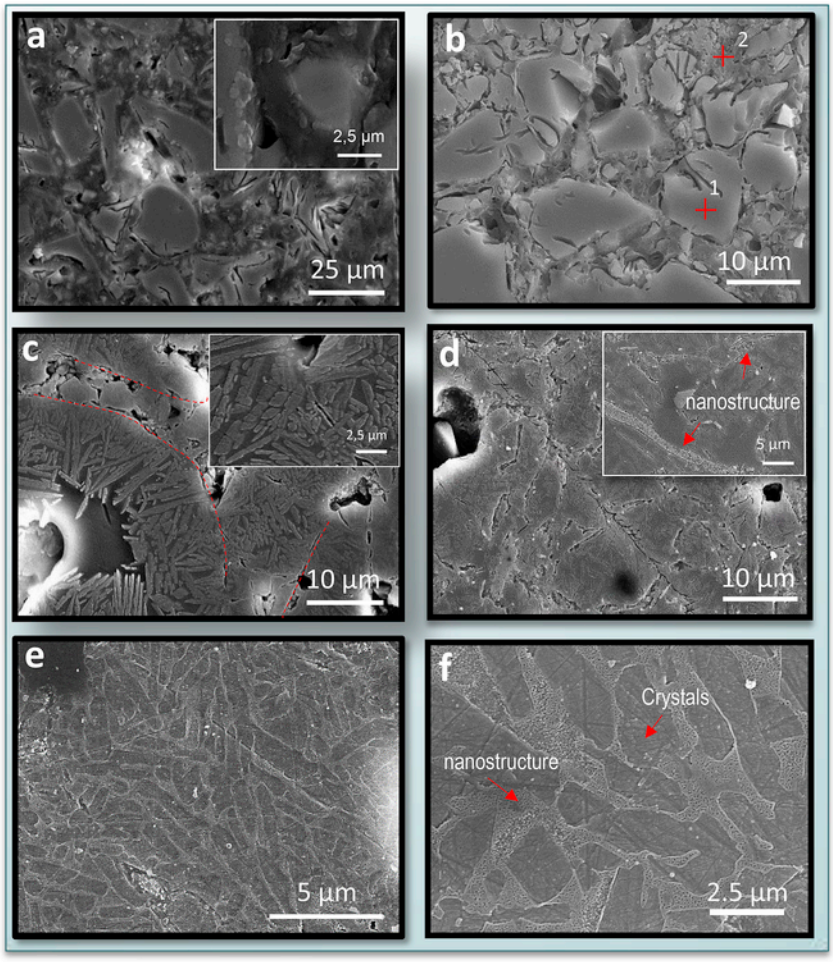

Fig. 3. FESEM micrographs at different magnifications of the Na-rich glass-ceramic feldspar quenched at a) 800 °C; b) 900 °C; c) 1100 °C; d) 1220 °C. In e), f) and sintered at 1220 °C with a dwell time of 6 min.

1045) and tetragonal SiO_2 (JCPDS card no. 00-013-0026). Finally, for quenched sample treated at 1220 °C, the XRD pattern is very similar to the one quenched at 1100 °C, however the diffraction peak intensities increase, which indicates crystal growth. In the XRD pattern of the sample sintered at 1220 °C 6 min it is possible to observe the Na-rich plagioclase diffraction pattern with higher crystallinity. In a Na-rich plagioclase (a solid solution between albite and anorthite), albite is the major phase (>50%) and anorthite appears in less content. Therefore, it is easy to conclude that the Na-rich plagioclase crystallization starts at temperatures >900 °C, and the crystallinity of the sample rises with the temperature increase, reducing, in consequence, the glassy phase content in the sample.

FESEM micrographs (Fig. 3a–f) corroborate the information extracted from XRD and can also provide more information about nucleation and crystallization. Fig. 3a shows the sample quenched at 800 °C where the frit grains are still visible, with sizes up to 20 µm. The frit grains are surrounded by a glassy phase formed from the reaction of the metakaolin and the frit. Therefore, at this temperature the feldspar structure has not crystallized yet. At 900 °C (Fig. 3b), the structure becomes slightly more homogeneous and the frit reacts locally with the surrounding glassy phase. As temperature increases, the reaction of metakaolin with the frit particles produces the diffusion of the necessary cations to form the albite-rich feldspar. An EDX analysis was carried out in this sample in order to understand the composition distribution. In Fig. 3b, two points are marked where the analysis was carried out, a frit grain (point 1) and a vitreous region (point 2). The composition distribution is presented in Table 2, in terms of equivalent oxides. As seen, the Al_2O_3 and SiO_2 percentages indicate the presence of silicoaluminates in the surrounding glassy phase. However, the relevant information is given by the percentages of Na, Ca and Sr. The amount of Ca is very similar in both regions (points 1 and 2), nevertheless, the amount of Na and Sr varies. In the frit grain the amounts of Na and Sr are larger than in the surrounded liquid phase, indicating the cations competence between both elements: Sr^{2+} begins to replace Na^+ in the feldspar structure due to a greater electronic affinity, releasing Na cations from the glassy phase, which will tend to create albite-rich crystals, as it was discussed above.

Table 2
Composition in equivalent oxides of the albite-rich glass quenched at 900 °C, obtained from EDX analysis.

	Na_2O	MgO	Al_2O_3	SiO_2	K_2O	CaO	ZnO	SrO	ZrO_2
Frit region (Point 1)	2.99	0.86	18.06	56.21	0.82	7.60	1.03	7.34	5.10
Glassy region (Point 2)	1.97	0.44	20.79	61.58	1.64	7.88	–	4.81	0.88

Fig. 3c shows the microstructure formed at 1100 °C (crystallization region in hot stage microscopy curve), where long albite-rich crystals (up to 10 μm) have been formed inside the frit grains thanks to release of Na^+ cations in the previous step, according to the XRD results. These albite-rich crystals grow in radial direction inside the former frit grain, due to a high nucleation rate at the grain boundaries (marked with red dash lines in Fig. 3c). Therefore, the crystals growth is limited by the former frit grain size and it is also possible to observe glassy phase surrounding the formed microcrystals. When thermal treatment temperature reached up to 1220 °C (Fig. 3d), the boundaries between the former frit regions disappear and the microcrystals growth is more homogeneous. In addition, some nanostructures regions begin to appear as it can be seen in the inset of Fig. 3d, marked with red arrows. Fig. 3 e and f shows the micrographs at different magnifications of the glass-ceramic sintered at 1220 °C 6 min. As it may be seen a dual microstructure, long albite-rich microcrystals (≈5 μm) are homogeneously distributed in the sample, surrounded by nanocrystals regions) which isolate the micrograins. The glassy phase residue is located at the nanoregions.

The chemical composition used in this work (Table 1) possesses lower content of Na than Ca, which would lead to expect the formation of anorthite-rich feldspar instead of albite-rich one. However, the main phase obtained in this material corresponds to a sodic plagioclase, in which albite is the major crystalline phase, as previously supported by the XRD patterns, Fig. 2. Moreover, the percentage of glassy phase, extracted from this XRD pattern by the diffraction software Bruker's Diffrac. Eva, is as low as ≈ 6%, which indicates the formation of a highly crystalline Na-rich feldspar glass-ceramic.

In this system, strontium probably acts as glass network disruptor, that is, the Sr^{2+} ions are introduced between Si/Al tetrahedra in Na^+ positions of the glass network system, where oxygen defects are more common, since its charge is electronically more compatible. Accordingly, during the sintering process, these sodium cations are available to form crystals, especially in areas around nucleating agents.

Thus, two conditions favor the formation of a Na-rich plagioclase with larger content of albite than anorthite crystals, despite the lower content of sodium in the frit composition: a) the albite and anorthite glass seeds; and b) Sr^{2+} cations acting as glass network disruptor, favouring the ejection of Na^{1+} cations from glassy matrix and the consequent crystallization of sodium-rich crystals, mainly due to a cationic competition. As known, cation diffusion in the melting liquid is quite relevant in the nucleation and crystallization processes, since the cations mobility influences the composition of the final crystals [4]. For this reason, as sodium ions have larger mobility than calcium ions, formation of a Na-rich plagioclase is favoured.

With the aim of obtaining a detailed phase and morphological characterization of the dual microstructure of glass-ceramic sintered at 1220 °C, TEM and HRTEM measurements were performed. In Fig. 4a it is observed a TEM image showing the presence of microcrystal and a nanostructured region having nanoparticles in a glassy matrix. The nanoparticles size is quite homogeneous with an average diameter between 30 and 40 nm. Fig. 4b illustrates a HRTEM image performed in the boundary between a microcrystal (top left corner) and glassy-phase of the nanostructured region. The microcrystal is perfectly crystalline and the corresponding FFT pattern is showed in Fig. 4c. The crystallographic planes are indexed and the spots have been identified as

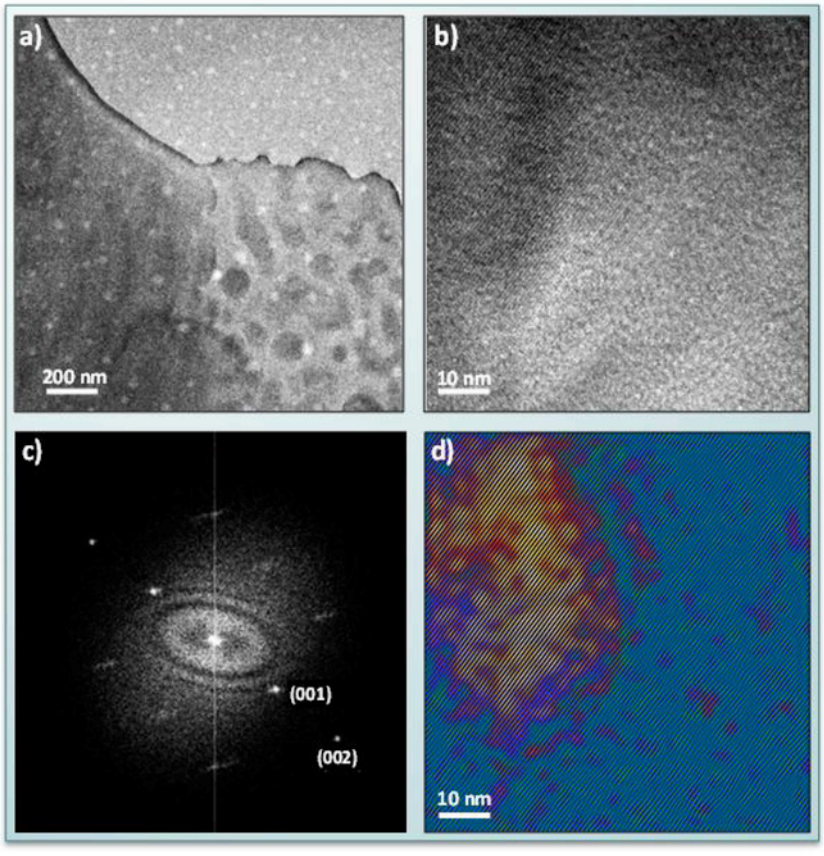

Fig. 4. a) TEM image of the Na-rich plagioclase glass-ceramic where nanoparticles/glassy matrix (right side) and a part of a microcrystal (left side) can be identified. **b)** HRTEM image of the interphase between the microcrystal and the glassy matrix. **c)** FFT microcrystal. The spots have been identified as (001) and (002) planes of an albite-rich structure. **d)** Inversed image achieved by selecting (001) and (002) spots of FFT image gathered on figure c). Yellow color represents zones with higher crystallinity while blue ones correspond to amorphous areas, where glassy phase is located. (For interpretation of the references to colour in this figure legend, the reader is referred to the Web version of this article.)

(001) with an interplanar distance of 0.6780 nm and (002) planes with an interplanar distance of 0.3391 nm. These determined values are slight higher than those for pure albite, i.e. 0.6387 nm for (001) and 0.3194 nm for (002) [23]. This experimental data correlated with the existence of calcium and strontium in the Na-rich plagioclase structure that is responsible for the distortion of crystallographic planes. To observe the limits of the crystalized region, and inverse mask has been applied to the FFT image, selecting the (001) and (002) spots (Fig. 4c). Yellow colour in Fig. 4d represents zones with higher crystallinity while blue ones correspond to amorphous areas, where glassy-phase is located. A chemical disaggregation of the crystalline feldspar it is observed at the interphase in which Si/Al tetrahedral ring of the feldspar structure by breaking the structure in the basal plane perpendicular to the (001) crystalline direction. This fact allows explaining the dual microstructure formation mechanism as follow: during sintering process, elongated microcrystals start nucleating at 1100 °C (as it was observed by quenching experiments in Fig. 3). Microcrystals initially have straight edges, however glassy phase begins etching differentially the grain edges, which lead to form irregular curved edges (Fig. 3e and f) after being completed the sintering cycle. Finally, the nanoparticles nucleated in the surrounding glassy-phase due the compositional enrichment.

Therefore, according to these results, it is possible to conclude that albite-rich crystals are formed at temperatures >900 °C, at which they still coexist with large amount of glassy phase that favors the cations diffusion. At 1100 °C long albite-rich crystals with straight edges are nucleated inside the frit grains, while glassy phase is surrounding them. Such crystals start being dissolved by glassy phase, forming irregular curved edges. Then, the nucleation of this glassy phase begins to form the nanoregions at ≈1220 °C around the microcrystals. These nanoregions continue growing and propagating throughout the sample during the dwell period, and probably during the cooling, which leads to the formation of the dual microstructure observed in the sample subjected to the complete sintering cycle. Moreover, the glassy phase has been reduced to 6%, forming a highly crystalline albite-rich glass-ceramic. In addition, the nanoregions located around the crystals stop its growth during the cooling process, obtaining crystals with lower sizes, as seen in Fig. 3 e and f.

3.2. X-ray photoelectron spectroscopy (XPS) measurements

XPS gives information about the composition, chemical and electronic state of the element present in the material surface. However, in this work, samples were polished before measuring in order to be able to study the internal structure of the glass-ceramics and the formation reactions. Fig. 5 shows the high resolution XPS spectra of Al 2p (Fig. 5 a, b and c) and Si 2p (Fig. 5d, e and f) of Na-rich plagioclase glass-ceramic sintered at 1220 °C, both quenched and with 6 min dwelling, respectively. Fig. 5a presents the comparison of Al 2p signal of both samples having similar binding energy, which agrees well with typical values of sodium and calcium aluminosilicate feldspars (74.1–74.4 eV) [24,25], although binding energy for Al 2p signal slightly shifted (0.05 eV) in vitreous network. Fig. 5b and c shows the deconvolution of the Al2p signal for the quenched sample and the sintered one at 1220 °C 6 min, respectively, where it is observed two main contributions corresponding to the aluminosilicate bindings (~74.20 eV) and the octahedral aluminum oxide (~74.60 eV) [24,26]. The XPS spectra indicate that quenched glass-ceramic possesses larger contribution of oxide bindings (Al—O) than glass-ceramic sintered with a dwelling time of 6 min. These results corroborate that crystallization progress during the dwelling temperature and the cooling step of the sample. This larger contribution of aluminum oxide in the quenched Na-rich plagioclase may be related to the binding energy shifting of the total contribution of Al 2p signal. Additionally, there is a strong relationship between the coordination number of Al and the binding energy, that is, as larger the coordination number is, higher the binding energy will be. For this reason, octahedral aluminum oxide with a coordination number of 6, has larger binding energy than Al 2p signal in tetrahedra of $NaAlSi_3O_8$ and in lesser extent of $CaAl_2Si_2O_8$, where Al has coordination number of 4.

In the case of Si 2p signal, both the quenched and the sintered samples also possess similar binding energies (Fig. 5d). The deconvoluted spectra (Fig. 5e and f) show two main contributions associated with albite feldspar at 102.6 eV and with tetrahedral Si—O at 102.3 eV [27]. Both contributions are similar in relative proportion, which indicates

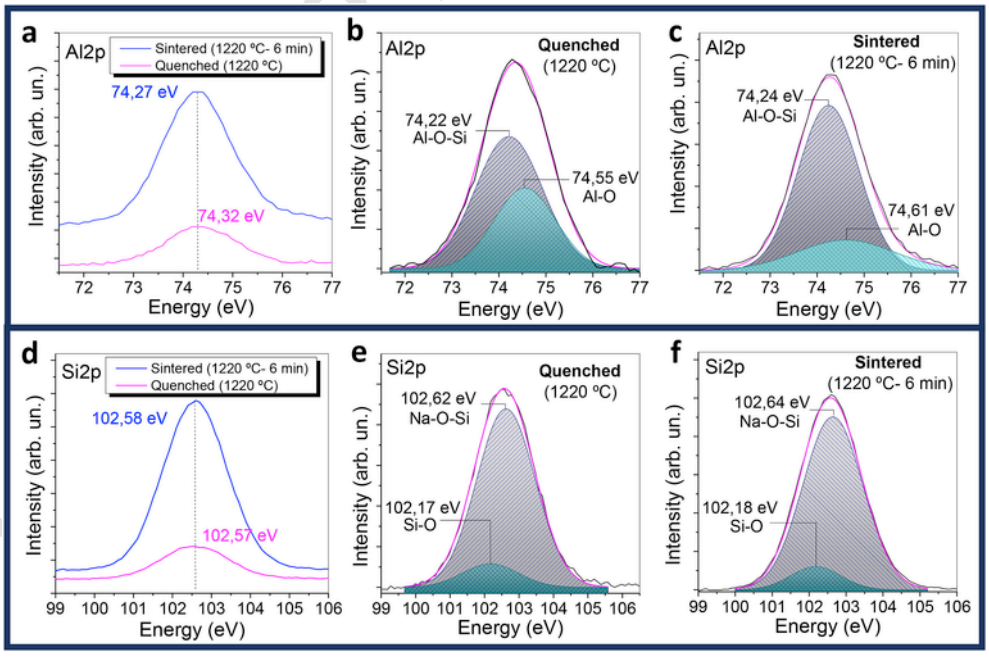

Fig. 5. High resolution XPS spectra of Al 2p (**a**, **b** and **c**) and Si 2p (**d**, **e** and **f**) for Na-rich plagioclase glass-ceramic sintered at 1220 °C, quenched or with a dwell time of 6 min. Deconvolution of each spectrum is shown in **b** and **e** for the complete sintered glass-ceramic and in **c** and **f** for quenched glass-ceramic.

that the major part of Si bonds corresponds to the formation of the Na-rich plagioclase feldspar and a small part to tetrahedral Si, probably corresponding to the glassy phase. Therefore, the Na—O—Si formation does not be largely affected by the quenching process, being formed these bonds before the cooling process of the thermal treatment. Signal position of main chemical species and FWHM for the XPS spectra are summarized in Table 3.

Fig. 6 shows high resolution XPS spectra of O 1s (Fig. 6 a and b) and Na1s (Fig. 6 c and d) for Na-rich plagioclase sintered at 1220 °C, quenched and with a dwell time of 6 min. In Fig. 6a it is observed a single peak for O 1s in both samples, however, lower binding energy (531.34 eV) is registered in quenched sample regarding the 6 min sintered (531.64 eV). In addition, the FWHM of these samples also evolves, being wider in the 6 min sintered glass-ceramic. These changes are related with oxygen coordination environments in each structure, being narrower when oxygen coordination is lower [26,28].

In the sodium aluminosilicate system, it is possible to find three components of O 1s signal, that is, three different oxygen environments, corresponding to Si—O—Si (~533 eV), Si—O—Al (~532 eV) and Si—O—Na (~531 eV). Fig. 6b shows the deconvolution of the O 1s signal in these 3 components for each sample, where it is possible to observe that the Si—O—Si bond suppose a low contribution in the system, since the main contribution is due to the Si—O—Al and Si—O—Na bonds. Sintered glass-ceramic at 1220 °C 6 min possesses larger proportion of Si—O—Na bonds than the quenched sample, which indicates higher crystallization of the Na-rich feldspar, and a wider FWHM, Table 3. This is also reflected in the chemical shift to lower binding energies of the quenched plagioclase, that indicates weaker bonds and therefore, lower feldspar crystallization. Fig. 5c shows the XPS spectra of Na 1s signal of both samples, where it is observed a significant shift to lower binding energies (0.74 eV) for quenched sample. This energy binding shift corroborates the nature of bonds and the crystallinity of the sample, that is, disorder structures as glass has lower binding energies than ordered crystalline phases. In addition, samples with non-bridging oxygens (NBO) also present lower binding energies. In Fig. 6d it is shown the deconvolution of the Na 1s peak, resulting two main contributions, one corresponding to the NBO (lower energies) and another one corresponding to modifying Na ions needed for charge balance during the process (higher energies) [29]. The Na 1s signal is placed in albite feldspars at 1072 eV [30,31], therefore, the albite-rich glass-ceramic sintered at 1220 °C 1 h fit this binding energy due to its higher crystallization, in comparison with the quenched sample that is a glassy phase, as it was discussed in section 3.2.

Therefore, as conclusions, XPS spectra of both samples with different thermal treatments present similar Al 2p and Si 2p binding energies and FWHM, indicating the formation of a sodium-rich aluminosilicates in both compounds, although Al 2p signal reveals larger amount of aluminosilicate bonds in the 1220 °C 6 min sintered sample. In case of O 1s and Na 1s signals, the binding energy is lower and the FWHM is shorter for quenched sample in comparison with sintered samples, indicating lower crystallinity and higher non-bridging bonds. These results suggest that the formation of the albite glass-ceramic, with high feldspar crystallinity requires a dwell sintering time and the cooling process to obtain both the dual microstructure and the high crystallinity.

3.3. NMR characterization

With the aim of deepening in the crystallization process undergone by the glass-ceramic and obtaining more precise information at short range, both compositionally and about order/disorder studies of the sintered feldspars NMR measurements were carried out.

^{29}Si has spin 1/2 and therefore does not suffer quadrupolar interactions, which makes it suitable to obtain information about electronic environment around Si sites. Fig. 6 shows the ^{29}Si NMR spectrum for the precursor frit (Fig. 7a), the quenched glass-ceramic at 1220 °C (Fig. 7b) and the sintered glass-ceramic at 1220 °C 6 min (Fig. 7c). ^{29}Si NMR spectrum of the frit exhibits a broad band in the range from −65 to −125 ppm with a maximum at ~ -92 ppm. This fact indicates that the frit might be mainly formed by a non-ordered calcium aluminosilicate in a glass structure having a Si/Al ratio between 1 and 2 [32]. Spectrum deconvolution allows distinguishing the different polymerization state in which silicon is found in the glass network. Peak positions are tabulated in Table 4 as well as the area contribution of each one and the corresponding Q_n species involved. Several works show that tetrahedra in glasses appear in more than one polymerization state, as occurs in our case [33]. Chemical shift values in the range from −66 to

Table 3
Signal position of main chemical species and full width at half maximum (FWHM) of XPS spectra for both Na-rich plagioclase, sintered at 1220 °C, quenched and 6 min.

Sample sintered at 1220 °C	Al 2p		Si 2p		O 1s		Na 1s	
	Position (eV)	FWHM (eV)	Position (eV)	FWHM (eV)	Position (eV)	FWHM (eV)	Position (eV)	FWHM (eV)
Quenched	74.32	1.64	102.57	1.99	531.34	2.28	1070.83	1.81
6 min	74.27	1.64	102.58	1.93	531.64	2.35	1071.57	1.96

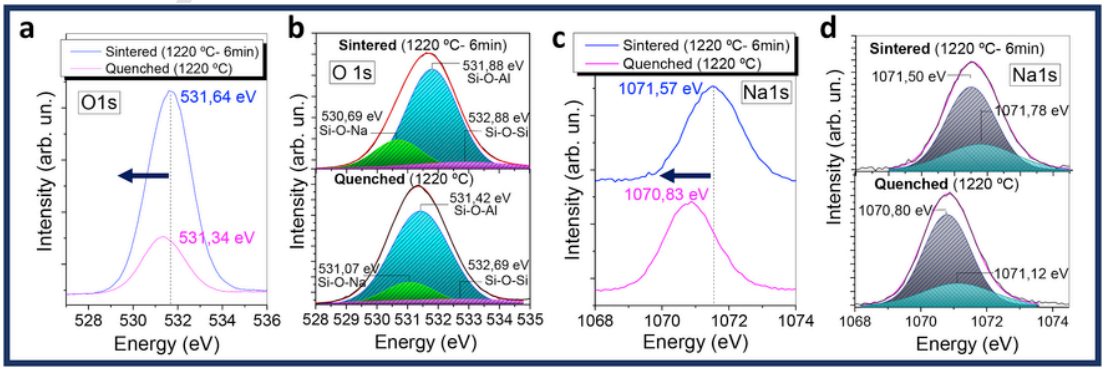

Fig. 6. High resolution XPS spectra of O 1s (**a** and **b**) and Ca 2p (**c** and **d**) for Na-rich plagioclase glass-ceramic sintered at 1220 °C, quenched or with a dwell time of 6 min. The corresponding deconvolution of each spectrum for both samples is shown in **b)** and **d)**.

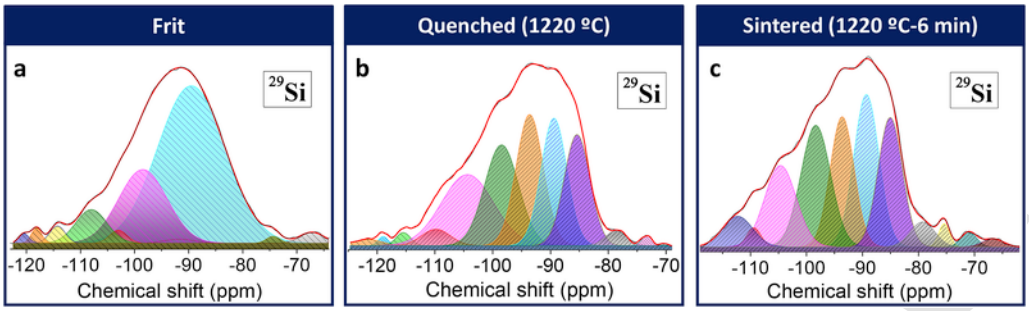

Fig. 7. ^{29}Si NMR spectra for **a)** the precursor frit; **b)** the quenched glass-ceramic at 1220 °C and **c)** the sintered glass-ceramic at 1220 °C 6 min. Deconvolution of ^{29}Si NMR spectrum of the frit shows the different polymerization state of Q_n units according to assignment of Table 4. In the case of quenched and sintered glass-ceramic, b) and c) respectively, the different Si neighbours are obtained and detailed in Table 5.

−74 ppm are assigned to Q_0 units in the ^{29}Si NMR spectrum. ^{29}Si NMR bands in the range −75 to −82 ppm correspond to Q_1 units and in the range −84 to −86 ppm correspond to Q_2 units. Q_3 units appear in the range of −90 to −101 ppm, while Q_4 groups provide ^{29}Si NMR peaks in the range from −103 to −120 ppm [34,35]. The area for each ^{29}Si NMR peak (Table 4) indicates that Q_3 species dominate the spectra, contributing with more than 85% of the total area.

In the plagioclase solid solution, the ordered end members, low albite and anorthite, have three resolved peaks in the ^{29}Si NMR spectrum, corresponding to T_{1m},T_{20} and T_{2m} tetrahedral sites [36]. Generally, ^{29}Si NMR peaks in the range from −81 ppm to −92 ppm are characteristic of anorthite structure while peaks in the range from −92 ppm to −112 ppm are associated to low albite structure [37]. ^{29}Si NMR spectrum for 1220 °C sintered 6 min and quenched glass-ceramic exhibit a broad band approximately covering the ranges of −60 to −120 ppm and −70 to −125 ppm, respectively, indicating, therefore, that both albite and anorthite structures contributes to these spectra. In order to analyze in detail, ^{29}Si NMR spectra for both samples, deconvolution was carried out and the ^{29}Si NMR peaks were tabulated in Table 5. Area contribution of each one and the corresponding assignment are also included in the table.

In Fig. 7c, it might be observed the presence of five prominent peaks for the 1220 °C 6 min sintered glass-ceramic associated to Q_4 units and another six minor bands placed at both extremes of the spectrum. ^{29}Si NMR peak at ~ -85 ppm is associated to Q_4(4Al), typical of anorthite-like sites [36,37]. ^{29}Si NMR peak at ~ -89 ppm is also usually associated to Q_4(4Al) sites but overlaps with T_2(3Al) site of albitic structures, typically placed in the −87 to −91 ppm range in plagioclases [37]. The rest of main peaks placed at −93.6, −98.3, −104.6 ppm matches well with albite-like sites corresponding to T_{2m} (2Si, 2Al), T_{20} (3Si, 1Al) and T_{1m} (3Si, 1Al) positions, respectively [36–38]. In general, chemical shifts are strongly affected by composition [37]; thus, taking into account chemical shifts reported in the literature for different plagioclases [36] and peak positions obtained in this work (see Table 4), it may be concluded that the glass-ceramic synthetized is a sodic plagioclase with a composition between an oligoclase (> An23) and labradorite (An < 50) [36].Moreover, it is worth mentioning that chemical shifts may slightly differ from reported values because of the presence of some amount of Si/Al disorder and other elements in the starting frit, as strontium and in lesser extent potassium, which distortion the lattice, change bond distances and thus modify resonances. For this reason, composition might not be exactly defined. Considering the results previously discussed and that the area contribution of the peak at ~ −89 ppm is ~20%, the most prominent one, it is highly probable that this resonance, principally correspond to T_2(3Al) site of albite structure although a small contribution of Q_4(4Al) sites may also take place, overlapping it. Besides, another ^{29}Si NMR peak less intense associated to an albite-like site is found at −112.3 ppm, corresponding to T_1(0Al) site. Triclinic albite has four crystallographic non-equivalent

Table 4
Chemical shift (ppm), area contribution (%) and Q_n unit assignment for each deconvoluted band of the^{29}Si NMR spectrum for the frit, plotted in Fig. 7a.

Chemical shift (ppm)	Area contribution (%)	Q_n unit assignment
−67.1	1.6	Q_0
−73.9	0.6	Q_0
−89.5	64.5	Q_3
−91.7	0.7	Q_3
−98.5	21.6	Q_3
−103.0	1.4	Q_4
−108.0	6.4	Q_4
−114.3	1.6	Q_4
−118.1	1.0	Q_4
−120.5	0.6	Q_4

Table 5
Chemical shift (ppm), area contribution (%) and site assignment for each deconvoluted band of the^{29}Si NMR spectrum for the quenched glass-ceramic at 1220 °C and the sintered one at 1220 °C 6 min, plotted in Fig. 7b and c, respectively. Deconvoluted bands show the different Si neighbours in each sample. (*) indicates an anorthite-like site. Rest of tabulated positions between −89.3 ppm and −112.3 ppm corresponds to albite-like sites.

Quenched glass-ceramic		Sintered glass-ceramic		Site assignment
Chemical shift (ppm)	Area contribution (%)	Chemical shift (ppm)	Area contribution (%)	
–	–	−66.7	0.9	Q_0 unit (glass)
−70.3	0.1	−71.0	1.2	Q_0 unit (glass)
−73.3	0.6	–	–	Q_0 unit (glass)
–	–	−75.4	1.3	Q_1 unit (glass)
−78.6	1.7	−79.3	3.3	Q_1 unit (glass)
−85.4	15.8	−85.0	16.8	Q_4(4Al) (*)
−89.4	18.1	−89.3	20.5	T_2 (3Al)
−93.6	19.6	−93.6	16.7	T_{2m} (2Al)
−98.5	18.7	−98.3	19.2	T_{20} (1Al)
−104.4	20.3	−104.6	13.7	T_{1m} (1Al)
−109.8	2.6	−109.4	1.5	Q_4 unit (glass)
–	–	−112.3	4.9	T_1 (0Al)
−115.5	1.1	–	–	Q_4 unit (glass)
−119.0	0.5	–	–	Q_4 unit (glass)
−121.6	0.9	–	–	Q_4 unit (glass)

tetrahedral positions known as T_{10}, T_{1m}, T_{20}, and T_{2m}. In the most ordered state, low albite, Si is placed in T_{1m},T_{20} and T_{2m} sites while Al in T_{10} and ^{29}Si NMR spectrum exhibit three bands of equal intensity, as it was discussed before [37]. However, the presence of additional broader peaks in Fig. 7b, with different intensity and higher overlapping indicate that Si neighbours have changed regarding an ordered state [39]. Moreover, the presence of T_2(3Al) and T_1(0Al) sites in albite-like domains corroborate that a slight Si, Al disorder distribution is presented. The rest of the peaks tabulated give a small contribution to ^{29}Si NMR spectrum and might be associated to the parent glass, according to Table 4 and the previous discussion of Fig. 6a. It is noticed mainly the presence of Q_1 units with a whole area contribution of 4.6% and in lesser extent Q_0 and Q_4 species with an area contribution of 2.0% and 1.5% respectively (see Table 5).

Quenched sample (Fig. 7b) exhibits approximately the same resonances registered in the sintered glass-ceramic (Fig. 7c) except for the presence of Si in T_1(0Al) positions, which confirms that the Na-rich plagioclase structure is formed on the heating, as it was previously discussed in section 3.2. Moreover, it presents a slight lower occupancy in T_2(3Al) sites in addition to the lack of T_1 (0Al) sites, which suggest that once glass-ceramic is complete sintered, larger degree of Si/Al disorder is favoured. Disorder in feldspars may cause the formation of larger amount of structural defects as Al—O—$^-$Al or Si—O—Si linkages [40], two of the main luminescent centres in feldspars [41].Regarding glass site assignments, it is observed as the main area contribution is of Q_4 units, with a 5.1%, and in lesser extent Q_0 and Q_1 species, with 0.7% and 1.7%, respectively. However, in the sample complete sintered the main contribution is of Q_1 units, which clearly indicates that a reorganization of structural elements in the crystallized plagioclase lattice occurs during devitrification process.

In other works, it has been established that a change in the Si—O bond length of 0.001 Å produces difference in the chemical shift of ca. 1 ppm and a change of 1° in the Si—O–T (T = Si,Al) bond angle led to chemical shift changes of 0.3–0.9 ppm. Moreover, it can be established that the chemical shift observed between Si resonances indicates that, as expected, bonds are slightly modified after devitrification process on the cooling.

Thus, by means of NMR it is corroborated that a synthetic Na-rich plagioclase with low content of glassy phase and a certain Si, Al disorder have been obtained by means of compositional design and fast sintering treatment following a ceramic route. A sintering treatment at 1220 °C with a dwell time of 6 min and further cooling process, promotes a dual microstructure having a hierarchical ordering by combining devitrification of micro regions and high nucleation of crystals at the nanoregions. This unique microstructure opens the engineering of feldspar as high crystalline glass ceramic to tailor properties in which nanocrystal and microcrystal coexists.

4. Conclusions

In this work it is presented for the first time a synthetic Na-rich plagioclase glass-ceramic obtained by a conventional ceramic procedure. Both, the chemical composition, using Sr and Ca as nucleating agents, and a fast sintering process lead to develop a unique highly crystalline and dual micro-nanostructure glass-ceramic.

The crystallization process reveals that crystallization of the Na-rich plagioclase occurs in two steps. Firstly, microcrystals devitrify on heating, in the range of 900–1100 °C, while nanocrystals start nucleating at 1220 °C in the glassy regions between microcrystals. Sintering treatment at 1220 °C for 6 min is required to develop a higher presence of nanoparticles and therefore to obtain a hierarchical micro-nanostructure of the glass-ceramic. Finally, ^{29}Si NMR measurements mainly show the contribution of Q_4(nAl) albite-like sites and in lesser extent some glass and anorthite-like sites, corroborating the formation of a sodic plagioclase structure. Analysis of Si environments for quenched glass-ceramic at 1220 °C and sintered at 1220 °C 6 min reveal that Si is placed in T1(0Al) sites only for the sintered sample, which suggest an increase of Si/Al disorder at short range after thermal treatment because of a structural reorganization during devitrification process.

This work may serve as a reference for future works in the field of glass-ceramic, since it demonstrates as microstructure could be engineered through a suitable crystallization process, which might be applied in the future to other glass-ceramic materials in order to tailor functionalities.

Acknowledgments

The authors express their thanks to the MINECO project MAT2017-86450-C4-1-R, and project CDTI of CTV for their financial support. Dra. E. Enriquez is also indebted to MINECO for a ‘‘Torres Quevedo’’ contract (ref: PTQ-14-07289), which is co-financed with European Social Funds.

References

[1] S.P. Chaudhuri, Crystallization of glass of the system - SiO, K20(Na20) - a1203, Ceram. Int. 8 (1982) 27–33.
[2] T.A. Khabas, V.V. Klimova, S.I. Starosvetskiy, A.P. Vasilyeva, M.A. Zvigintsev, Crystal phase formation in colored leucite-reinforced glass-ceramics for dental restorations, Inorg. Mater. Appl. Res. 8 (2017) 186–193, https://doi.org/10.1134/S2075113317010191.
[3] W. Flehmig, The synthesis of feldspars at temperature between 0º-80º C, their ordering behaviour and twinning, Contrib. Mineral. Petrol. 65 (1977) 1–9.
[4] I. Parsons, Feldspars and Their Reactions, Springer. Science + Business Media, B.V., Edinburgh, 1994https://doi.org/10.1180/minmag.1995.059.397.23.
[5] J. Yuan, J. Yang, H. Ma, C. Liu, C. Zhao, Hydrothermal synthesis of analcime and hydroxycancrinite from K-feldspar in Na $_2$ SiO $_3$ solution: characterization and reaction mechanism, RSC Adv. 6 (2016) 54503–54509, https://doi.org/10.1039/C6RA08080D.
[6] E.S. Derkacheva, M.G. Krzhizhanovskaya, R.S. Bubnova, Thermal behavior of reedmergnerite NaBSi3O8 and searlesite NaBSi2O5(OH)2, Glas. Phys. Chem. 43 (2017) 459–463, https://doi.org/10.1134/S1087659617050030.
[7] S. Su, H. Ma, X. Chuan, Hydrothermal synthesis of zeolite A from K-feldspar and its crystallization mechanism, Adv. Powder Technol. 27 (2016) 139–144, https://doi.org/10.1016/j.apt.2015.11.011.
[8] E. Nyankson, J.K. Efavi, A. Yaya, G. Manu, K. Asare, R.Y. Abrokwah, Synthesis and characterisation of zeolite-A and Zn-exchanged zeolite-A based on natural aluminosilicates and their potential applications, Cogent Eng (2018) 200–202, https://doi.org/10.1080/23311916.2018.1440480.
[9] I. Buljan, C. Kosanovic, D. Kralj, A novel synthesis of nano-sized mullite from aluminosilicate precursors, J. Alloy. Comp. 509 (2011) 8256–8261, https://doi.org/10.1016/j.jallcom.2011.05.099.
[10] C. Liu, Epitaxy in the Crystallization of Feldspar Gels and Glasses, University Microfilms International, 1993https://doi.org/10.1557/PROC-346-721.
[11] T.Y. Sablina, N.L. Savchenko, A.G. Mel'nikov, S.N. Kul'kov, Vacuum sintering of a ceramic based on zirconium dioxide, Glas. Ceram 51 (1994) 198–201, https://doi.org/10.1007/BF00682584.
[12] C. Liu, S. Komarneni, R. Roy, Epitaxy in the crystallization of feldspar gels and glasses, MRS Proc 346 (1994) 721, https://doi.org/10.1557/PROC-346-721.
[13] C. Liu, S. Komarneni, R. Roy, Crystallization of anorthite-seeded albite glass by solid-state epitaxy, J. Am. Ceram. Soc. 75 (1992) 2665–2670, https://doi.org/10.1111/j.1151-2916.1992.tb05486.x.
[14] P.H. Ribbe, H.D. Megaw, W.H. Taylor, R.B. Ferguson, R.J. Traill, The albite structures, Acta Crystallogr. B 25 (1969) 1503–1518, https://doi.org/10.1107/S0567740869004262.
[15] U. Selvaraj, C.L. Liu, S. Komarneni, R. Roy, Epitaxial crystallization of seeded albite glass, J. Am. Ceram. Soc. 74 (1991) 1378–1381, https://doi.org/10.1111/j.1151-2916.1991.tb04115.x.
[16] V. Fuertes, M.J. Cabrera, J. Seores, D. Muñoz, J.F. Fernández, E. Enríquez, Hierarchical micro-nanostructured albite-based glass-ceramic for high dielectric strength insulators, J. Eur. Ceram. Soc. (2018) https://doi.org/10.1016/j.jeurceramsoc.2018.02.009.
[17] V. Fuertes, M.J. Cabrera, J. Seores, D. Muñoz, J.F. Fernández, E. Enríquez, Enhanced Wear Resistance of Engineered Glass-Ceramic by Nanostructured Self-Lubrication, Submitted. (n.d.).
[18] J.J. Reinosa, D.M.Y. Marero, A. Del Campo, M.Á. De La Rubia, J.F. Fernández, Chemical analysis with high spatial resolution by rutherford backscattering and Raman Confocal spectroscopies: surface hierarchically structured glasses, J. Am. Ceram. Soc. 96 (2013) 1783–1788, https://doi.org/10.1111/jace.12397.
[19] J.J. Reinosa, F. Rubio-Marcos, E. Solera, M.A. Bengochea, J.F. Fernández, Sintering behaviour of nanostructured glass-ceramic glazes, Ceram. Int. 36 (2010) 1845–1850, https://doi.org/10.1016/j.ceramint.2010.03.029.

[20] D.O. Obada, D. Dodoo-Arhin, M. Dauda, F.O. Anafi, A.S. Ahmed, O.A. Ajayi, The impact of kaolin dehydroxylation on the porosity and mechanical integrity of kaolin based ceramics using different pore formers, Results Phys 7 (2017) 2718–2727, https://doi.org/10.1016/j.rinp.2017.07.048.
[21] L. Carbajal, F. Rubio-Marcos, M.A. Bengochea, J.F. Fernandez, Properties related phase evolution in porcelain ceramics, J. Eur. Ceram. Soc. 27 (2007) 4065–4069, https://doi.org/10.1016/j.jeurceramsoc.2007.02.096.
[22] J.J. Reinosa, B. García-Baños, J.M. Catalá-Civera, J.F. Fernández, A step ahead on efficient microwave heating for kaolinite, Appl. Clay Sci. 168 (2019) 237–243, https://doi.org/10.1016/j.clay.2018.11.001.
[23] P.H. Ribbe, H.D. Megaw, W.H. Taylor, R.B. Ferguson, R.J. Traill, The albite structures, Acta Crystallogr. Sect. B Struct. Crystallogr. Cryst. Chem. 25 (1969) 1503–1518, https://doi.org/10.1107/S0567740869004262.
[24] J. Wang, Z. Wang, L. Yang, G. Yang, C. Miao, P. Lv, Natural albite as a novel solid basic catalyst for the effective synthesis of biodiesel: characteristics and performance, Energy (2017) https://doi.org/10.1016/j.energy.2017.11.086.
[25] R. Golovchak, M.J. Davis, P. Vullo, A. Astashkin, L. Nichols, A. Ingram, H. Jain, The Charge State of Titanium Ions in Pd-Doped Ti : CMAS Glass and Glass-Ceramics, 20172568–2581, https://doi.org/10.1111/jace.14791.
[26] M. Todea, E. Vanea, S. Bran, P. Berce, S. Simon, XPS analysis of aluminosilicate microspheres bioactivity tested in vitro, Appl. Surf. Sci. 270 (2013) 777–783, https://doi.org/10.1016/j.apsusc.2013.01.178.
[27] X. Cui, Y. Cheng, H. Lin, F. Huang, Q. Wu, Y. Wang, Size-dependent abnormal thermo-enhanced luminescence of ytterbium-doped nanoparticles, Nanoscale (2017) https://doi.org/10.1039/C7NR04575A.
[28] M.F. Hochella, G.E. Brown, Aspects of silicate surface and bulk structure analysis using X-ray photoelectron spectroscopy (XPS), Geochem. Cosmochim. Acta 52 (1988) 1641–1648, https://doi.org/10.1016/0016-7037(88)90232-3.
[29] H. Bach, D. Krause, Analysis of the Composition and Structure of Glass and Glass Ceramics, Springer Science & Business Media, Mainz, Germany, 2014.
[30] H. Seyama, M. Soma, X-ray photoelectron spectroscopic study of the effect of heating on montmorillonite containing sodium and potassium cations, Clay Clay Miner. 34 (1986) 672–676.
[31] W. Wang, J. Cong, J. Deng, X. Weng, Y. Lin, Y. Huang, Developing effective separation of feldspar and quartz while recycling tailwater by HF pretreatment, Minerals 8 (2018) 1–15, https://doi.org/10.3390/min8040149.
[32] S. Lee, J. Stebbins, The degree of aluminum avoidance in aluminum silicate glasses, Am. Mineral. 84 (1999) 937–945, https://doi.org/10.2138/am-1999-5-630.
[33] A.R. Allu, S. Balaji, D.U. Tulyaganov, G.C. Mather, F. Margit, M.J. Pascual, R. Siegel, W. Milius, J. Senker, D.A. Agarkov, V.V. Kharton, J.M.F. Ferreira, Understanding the formation of CaAl2Si2O8 in melilite-based glass-ceramics: combined diffraction and spectroscopic studies, ACS Omega 2 (2017) 6233–6243, https://doi.org/10.1021/acsomega.7b00598.
[34] O. V Filonenko, V.S. Kuts, M.I. Terebinska, V. V Lobanov, Quantum chemical calculation of 29Si NMR spectrum of silicone dioxide fullerene-like molecules, Chem. Phys. Technol. Surf. 6 (2015) 263–268, https://doi.org/10.15407/hftp06.02.263.
[35] K.J.D. MacKenzie, E.S. Mark, Multinuclear Solid-State NMR of Inorganic Materials, 2002.
[36] R.J. Kirkpatrick, R.A. Kinsey, K.A. Smith, D.M. Henderson, E. Oldfields, High resolution solid-state sodium-23 , aluminum-27 , and silicon-29 nuclear magnetic resonance spectroscopic reconnaissance of alkali and plagioclase feldspars, Am. Mineral. 70 (1985) 106–123.
[37] R.J. Kirkpatrick, M.A. Carpenter, W.H. Yang, B. Montez, 29Si magic-angle NMR spectroscopy of low-temperature ordered plagioclase feldspars, Nature 325 (1987) 236–238, https://doi.org/10.1038/325236a0.
[38] W.H. Yang, R.J. Kirkpatrick, D.M. Henderson, High-resolution 29Si, 27Al and 23Na NMR spectroscopic study of Al-Si disordering in annealed albite and oligoclase, Am. Mineral. 71 (1986) 712–726.
[39] L. Sanchez-Muñoz, L. Nistor, G. Van Tendeloo, J. Sanz, Modulated structures in KAlSi3O8: a study by high resolution electron microscopy and 29Si MAS-NMR spectroscopy, J. Electron. Microsc. 47 (1998) 17–28, https://doi.org/10.1093/oxfordjournals.jmicro.a023555.
[40] Andrew Putnis, The crystal structure of minerals II- silicates, In: An Introd. to Miner. Sci, 1992, pp. 141–184, https://doi.org/10.1017/CBO9781139170383.
[41] M. Pagel, V. Barbin, P. Blanc, D. Ohnenstetter, Cathodoluminescence in Geosciences, Springer-Verlag Berlin Heidelberg GmgH, New York, 2000.